Enzymatic removal of ribonucleotides from DNA is essential for Mammalian genome integrity and development

Cell

Enzymatic Removal of Ribonucleotides from DNA Is Essential for Mammalian Genome Integrity and Development

Martin A.M. Reijns,[1,3] Björn Rabe,[1,3] Rachel E. Rigby,[1] Pleasantine Mill,[1] Katy R. Astell,[1] Laura A. Lettice,[1] Shelagh Boyle,[1] Andrea Leitch,[1] Margaret Keighren,[1] Fiona Kilanowski,[1] Paul S. Devenney,[1] David Sexton,[1] Graeme Grimes,[1] Ian J. Holt,[2] Robert E. Hill,[1] Martin S. Taylor,[1] Kirstie A. Lawson,[1] Julia R. Dorin,[1] and Andrew P. Jackson[1,*]

[1]Medical Research Council Human Genetics Unit, MRC Institute of Genetics and Molecular Medicine, University of Edinburgh, Edinburgh EH4 2XU, UK

[2]Medical Research Council Mitochondrial Biology Unit, Cambridge CB2 0XY, UK

[3]These authors contributed equally to this work

*Correspondence: andrew.jackson@igmm.ed.ac.uk

DOI 10.1016/j.cell.2012.04.011

SUMMARY

The presence of ribonucleotides in genomic DNA is undesirable given their increased susceptibility to hydrolysis. Ribonuclease (RNase) H enzymes that recognize and process such embedded ribonucleotides are present in all domains of life. However, in unicellular organisms such as budding yeast, they are not required for viability or even efficient cellular proliferation, while in humans, RNase H2 hypomorphic mutations cause the neuroinflammatory disorder Aicardi-Goutières syndrome. Here, we report that RNase H2 is an essential enzyme in mice, required for embryonic growth from gastrulation onward. RNase H2 null embryos accumulate large numbers of single (or di-) ribonucleotides embedded in their genomic DNA (>1,000,000 per cell), resulting in genome instability and a p53-dependent DNA-damage response. Our findings establish RNase H2 as a key mammalian genome surveillance enzyme required for ribonucleotide removal and demonstrate that ribonucleotides are the most commonly occurring endogenous nucleotide base lesion in replicating cells.

INTRODUCTION

DNA is believed to have evolved from an ancestral RNA world as a more stable store of genetic information (Alberts et al., 2002; Cech, 2011). Ribonucleotides differ from deoxynucleotides by the presence of a single reactive hydroxyl group at the 2′ position of the ribose sugar, rendering RNA ~100,000-fold more susceptible to spontaneous hydrolysis under physiological conditions (Li and Breaker, 1999). The presence of ribonucleotides in genomic DNA is therefore undesirable, as it renders DNA more sensitive to strand breakage. It has long been thought that such misincorporation is prevented by the stringent selectivity of replicative DNA polymerases, favoring deoxynucleoside triphosphate (dNTP) over ribonucleoside triphosphate (rNTP) substrates (Joyce, 1997). However, recent in vitro experiments have demonstrated that, under physiologically relevant conditions in which rNTPs substantially exceed dNTPs, such DNA polymerases may incorporate a ribonucleotide base every few thousand base pairs (Nick McElhinny et al., 2010a). Budding yeast expressing a less selective replicative polymerase only displayed widespread ribonucleotide incorporation when ribonuclease (RNase) H2 activity was genetically abolished (Nick McElhinny et al., 2010b). This directly implicated RNase H2 in the removal of such ribonucleotides.

RNase H enzymes hydrolyze the RNA strand of RNA/DNA hybrids (Stein and Hausen, 1969). Such hybrids form during many cellular processes, including DNA replication (Machida et al., 1977), telomere elongation (Förstemann and Lingner, 2005), and transcription (Huertas and Aguilera, 2003; Li and Manley, 2005). Eukaryotes have two types of RNase H with distinct biochemical properties and substrate specificity (reviewed in Cerritelli and Crouch, 2009). RNase H1 is a processive monomeric enzyme that requires interaction with 2′-OH groups from four consecutive ribonucleotides for efficient substrate cleavage (Nowotny et al., 2007). Mammalian RNase H1 has two isoforms: a nuclear isoform of undefined function and a mitochondrial isoform that is essential for mitochondrial DNA replication (Cerritelli et al., 2003). However, the predominant source of RNase H activity in mammalian cells is RNase H2 (Büsen, 1980). Like RNase H1, it digests the RNA strand of RNA/DNA hybrids in a processive manner (Chon et al., 2009), but it also recognizes single ribonucleotides in a DNA duplex and cleaves the 5′-phosphodiester bond of the ribonucleotide (Eder et al., 1993). In eukaryotes, RNase H2 is a multimeric complex consisting of three subunits: RNASEH2A, RNASEH2B, and RNASEH2C (Crow et al., 2006a; Jeong et al., 2004). The RNASEH2A subunit contains the catalytic center, whereas the closely intertwined auxiliary RNASEH2B and C subunits are likely involved in interactions with other proteins (Figiel et al., 2011; Reijns et al., 2011; Shaban et al., 2010). A PIP box motif at the C terminus of the RNASEH2B subunit guides the interaction

between RNase H2 and PCNA (Chon et al., 2009) and its localization to replication foci (Bubeck et al., 2011), consistent with a role for the RNase H2 enzyme in DNA replication and/or repair.

Mutations in all three genes that encode the RNase H2 subunits cause the autosomal-recessive disorder Aicardi-Goutières syndrome (AGS) (Crow et al., 2006a). This early-onset neuroinflammatory condition mimics congenital viral infection and has immunological similarities to the autoimmune disease systemic lupus erythematosus (Ramantani et al., 2010). RNase H2 mutations that cause AGS result in partial rather than absolute loss of RNase H2 enzyme function (Reijns et al., 2011; Rice et al., 2007). Two further enzymes have been implicated in AGS: the 3′→5′ DNA exonuclease TREX1 (Crow et al., 2006b) and a dNTP triphosphohydrolase, SAMHD1 (Rice et al., 2009). Innate immune-mediated inflammation is thought to result from the accumulation of endogenous nucleic acid species that are usually degraded by these enzymes, e.g., during DNA replication/repair (Yang et al., 2007) or suppression of endogenous retroelements (Manel and Littman, 2011; Stetson et al., 2008).

The nucleic acids that may accumulate as a consequence of impaired RNase H2 function are yet to be defined, and although RNase H2 enzyme activity has been studied for more than 40 years (Stein and Hausen, 1969), its cellular functions are poorly understood. Initially, RNase H2 was proposed to act in removal of the RNA oligonucleotides that prime Okazaki fragment synthesis during lagging-strand replication. In vitro biochemical studies indicate that sequential action of RNase H2 and FEN1 are sufficient to complete this process (Goulian et al., 1990; Turchi et al., 1994). However, primer removal through flap processing by FEN1/DNA2 has become the predominant model for Okazaki fragment maturation (Burgers, 2009; Rossi and Bambara, 2006). RNase H2 may also be important for the resolution of R loops that arise during transcription (El Hage et al., 2010) or for the repression of endogenous retroelements (Cerritelli and Crouch, 2009). Finally, the distinctive property that allows RNase H2 to recognize and cleave single ribonucleotides that are embedded in DNA duplexes suggests a role in the removal of such nucleotides from genomic DNA (Rydberg and Game, 2002).

Here, we performed targeted mutagenesis of the mouse *Rnaseh2b* gene to gain insight into the in vivo role of the mammalian RNase H2 enzyme. Ablation of *Rnaseh2b* in mice leads to early embryonic lethality due to elevated DNA damage and reduced cellular proliferation during gastrulation. We establish that the growth arrest is the consequence of a p53-dependent DNA damage response associated with the accumulation of single ribonucleotides in genomic DNA. Thus, we demonstrate that removal of ribonucleotides to preserve genome integrity is an essential cellular function of RNase H2 in mammals.

RESULTS

Rnaseh2b Is a Developmentally Essential Gene

Rnaseh2b^{E202X} embryonic stem (ES) cells with a premature stop codon in exon 7 of *Rnaseh2b* were generated by targeted homologous recombination (Figure 1A). Correct recombination of both arms of the targeting cassette was confirmed by Southern blotting and long-range PCR (Figures 1A and 1B) and the presence of a nonsense mutation at codon 202 (E202X) established by sequencing (Figure 1C). ES cells were injected into C57BL/6J host blastocysts to generate germline chimeras and subsequently heterozygous *Rnaseh2b*$^{E202X/+}$ mice. Intercrossing of *Rnaseh2b*$^{E202X/+}$ animals failed to yield live-born homozygous null mice ($p < 0.001$; Figures 1D and 1E). Similarly, homozygotes were not present ($p < 0.001$) in litters of a second independent line, *Rnaseh2b*^{tm1a}, derived from EUCOMM "knockout-first" ES cells.

As no viable homozygous animals were obtained from either of these alleles, we concluded that *Rnaseh2b* was likely to be an essential gene that is required for embryonic viability. At embryonic day 6.5 (E6.5), *Rnaseh2b*$^{E202X/E202X}$ embryos were present at Mendelian ratios and were almost indistinguishable in size from wild-type littermates, suggesting normal progression of early embryogenesis (Figures 2A and 2B). However, by E7.5, there was a 23% and 32% decrease in embryonic height and width, respectively ($p < 0.005$; Figure 2B), suggesting a failure to increase the rate of proliferation in the epiblast that normally occurs at the onset of gastrulation (Mac Auley et al., 1993; Snow, 1977). Though all mutants proceeded through gastrulation, the embryos remained reduced in size and were developmentally retarded (Figure 2A). By E9.5 ($n = 23$), they were frequently truncated (57%) with few or very small postcervical somites (52%) and defects in allantois development (48%). At E10.5, histology demonstrated increased numbers of cells with condensed or fragmented nuclei, and at E11.5, a terminal phenotype was evident with loss of tissue morphology and integrity (data not shown).

Rnaseh2b^{E202X} Results in Absolute Loss of RNase H2 Complex Function

To examine the effect of the *Rnaseh2b*^{E202X} mutation on the RNase H2 enzyme, immunoblotting was performed with affinity-purified antibodies. As the premature stop codon is not in the final *Rnaseh2b* exon, it is expected to cause nonsense-mediated decay of the transcript. Consistent with this, we did not detect a truncated RNASEH2B^{E202X} protein (Figure S1B available online). Also, full-length RNASEH2A, B, and C subunits were all undetectable in E9.5 *Rnaseh2b*$^{E202X/E202X}$ embryo lysates (Figure 2C), indicating that RNASEH2B is required for in vivo stability of the heterotrimeric complex. Furthermore, type 2 RNase H activity against a DNA duplex oligonucleotide with an embedded ribonucleotide was undetectable in *Rnaseh2b*$^{E202X/E202X}$ embryos (Figure 2D). In contrast, general RNase H activity was retained, albeit at <10% of wild-type embryo levels (Figure 2D), consistent with retention of normal RNase H1 activity. Given that RNase H2 is absent from *Rnaseh2b*$^{E202X/E202X}$ embryos, we hereafter refer to these embryos and their derivative cells as RNaseH2^{null} and their genotype as *Rnaseh2b*$^{-/-}$. Significantly, such embryos entirely lack detectable enzyme activity against isolated ribonucleotides embedded in DNA.

RNase H2 Is Highly Expressed in Proliferating Cells

The anti-RNase H2 antibody specifically detected RNase H2 when used for immunofluorescence microscopy, as staining was absent in null embryos (Figures S2A and S2B). Endogenous

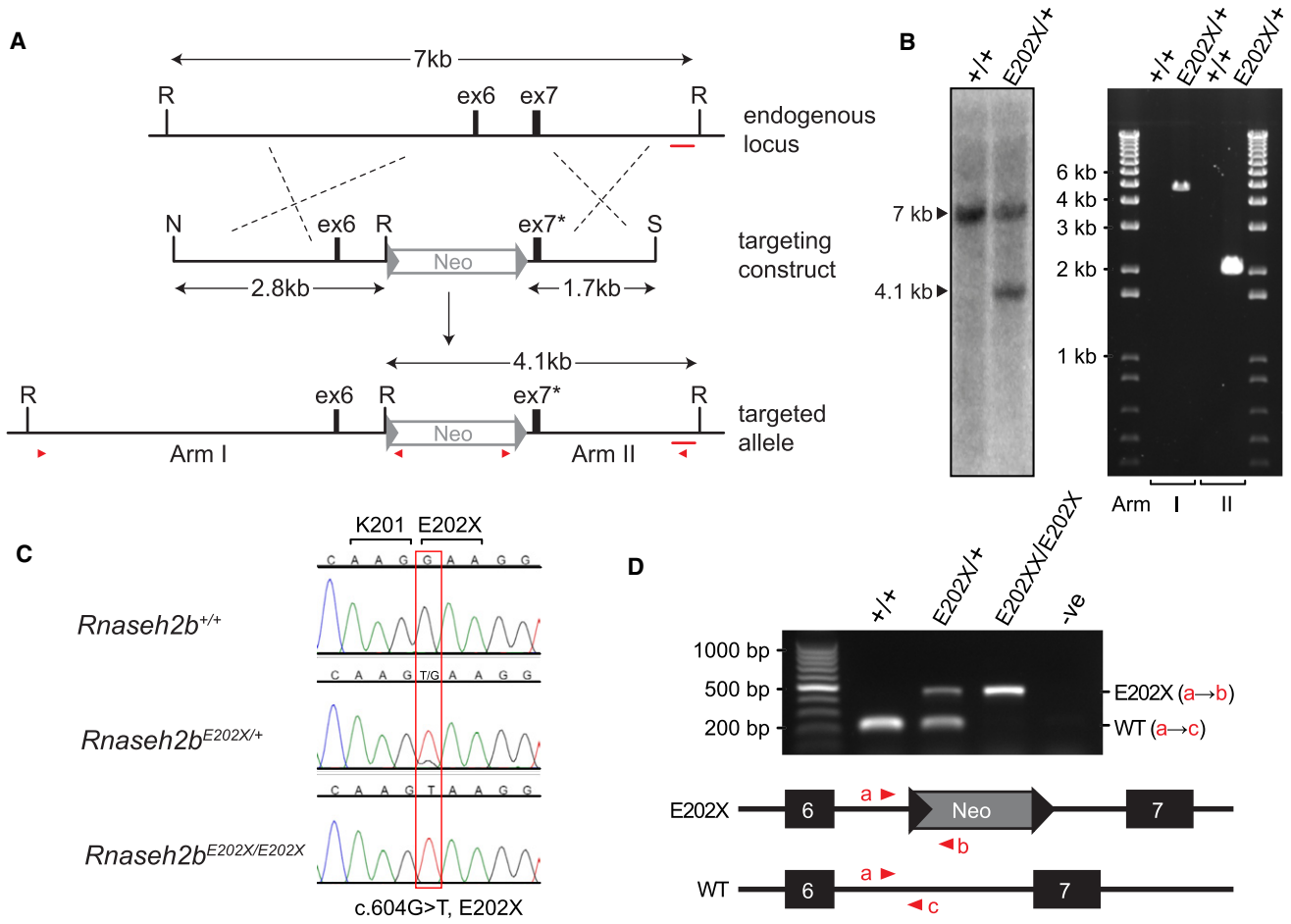

E

Mutant/Stage	+/+	+/m	m/m	Total	χ^2 test
Liveborn pups					
Rnaseh2b^{E202X}	34% (104)	66% (206)	0% (0)	310	p<0.001
Rnaseh2b^{tm1a}	41% (22)	59% (32)	0% (0)	54	p<0.001
Staged dissections					
Rnaseh2b^{E202X}	+/+	+/m	m/m	Total	
E6.5	31% (12)	46% (18)	23% (9)	39	n.s.
E7.5	42% (24)	39% (22)	19% (11)	57	
E8.5	20% (13)	57% (38)	23% (15)	66	
E9.5	24% (19)	46% (36)	30% (24)	79	
E10.5	29% (9)	52% (16)	19% (6)	31	

Figure 1. Targeted Inactivation of the *Rnaseh2b* Gene Causes Embryonic Lethality

(A) Schematic depicting targeted mutagenesis of exon 7 of the *Rnaseh2b* gene. (Top) A 7 kb segment of the *Rnaseh2b* genomic locus; exons 6 (ex6) and 7 (ex7) are indicated by black boxes, flanked by EcoRI sites (R). (Middle) *Not*I (N)-Sal (S) restriction fragment of the final targeting construct, comprising 4.5 kb of genomic DNA and a Neomycin selection cassette (Neo) flanked by Cre recombinase loxP sites (triangles). (Bottom) Successfully targeted endogenous locus containing the mutagenized exon 7 (ex7*). Red arrowheads indicate primers used to amplify arm I and arm II to confirm correct targeting.

(B) Southern blotting and long-range PCR confirm successful targeting by homologous recombination. The introduction of an additional EcoRI site results in a restriction fragment of 4.1 kb detected on Southern blotting with the 400 bp probe (red bar in A) for the targeted ES cells (E202X/+) that is not present in parental DNA (+/+). Arm I (4.7 kb) and arm II (2.2 kb) fragments are amplified by PCR in correctly targeted ES cells only.

(C) Sequencing traces for *Rnaseh2b*$^{+/+}$, *Rnaseh2b*$^{E202X/+}$, and *Rnaseh2*$^{E202X/E202X}$ DNA show the introduced nonsense mutation (red box).

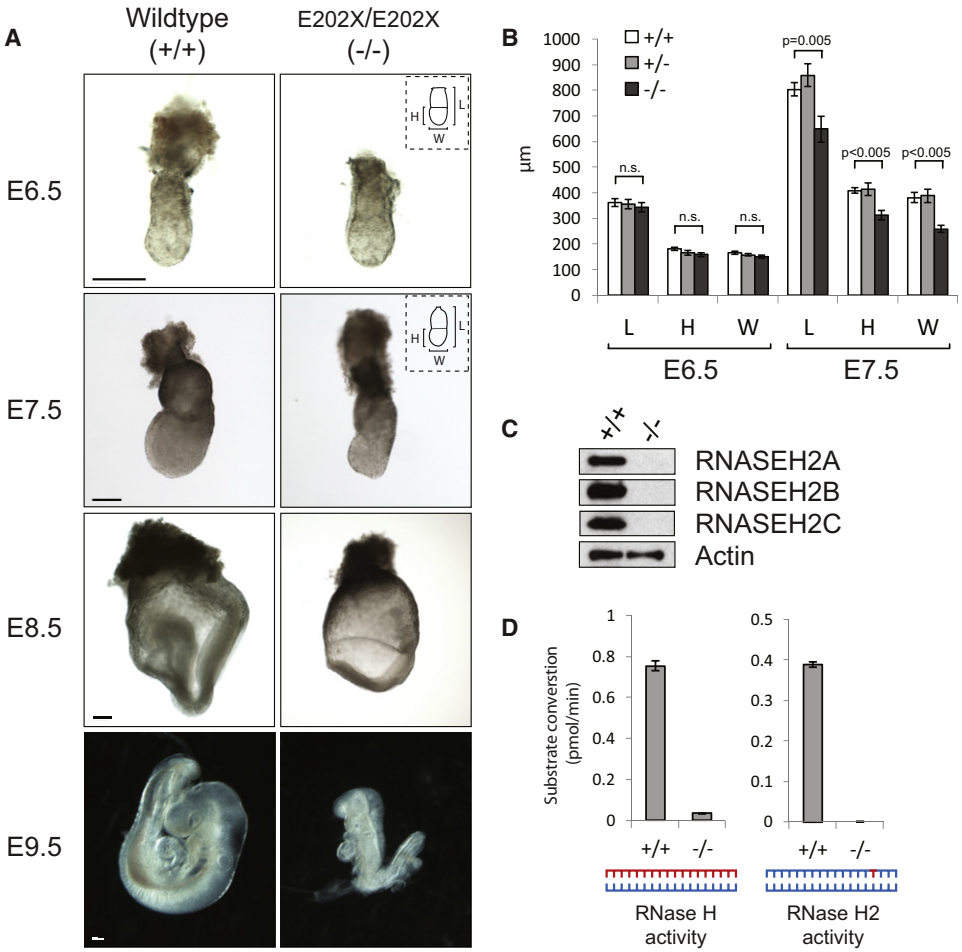

Figure 2. *Rnaseh2b*$^{E202X/E202X}$ Embryos Exhibit Severe Growth Failure during Early Development, Resulting in Embryonic Lethality

(A and B) Growth failure in mutant embryos starts at gastrulation.

(A) Photomicrographs of representative embryos from embryonic stages E6.5, E7.5, E8.5, and E9.5. Scale bars, 200 μm.

(B) There is a significant difference in length (L), width (W), and height (H) between wild-type (+/+) and mutant *Rnaseh2b*$^{E202X/E202X}$ embryos (denoted as −/−) at E7.5, but not at E6.5. (E7.5, 7 litters: n = 22,21,11; E6.5, 6 litters: n = 12,18,9 for +/+, +/−, and −/−, respectively). Error bars represent SEM; t test; n.s., not significant.

(C) Immunoblotting demonstrates that all three RNase H2 subunits (RNASEH2A, B, and C) are absent from mutant embryo lysates. Loading control, actin.

(D) Type 2 RNase H activity is undetectable in mutant embryos, and total cellular RNase H activity is reduced to < 10%. Cleavage of RNase H (RNA/DNA hybrid) and RNase H2-specific substrates by mutant and wild-type E9.5 embryo lysates was measured using fluorescence-based assays. Error bars represent SD. n = 3 replicates.

See also Figure S1.

RNase H2 exhibited nuclear localization in early embryos, consistent with proposed roles in DNA replication and repair. Expression was observed in blastocysts (Figure 3A) and in all three embryonic layers during gastrulation (Figure 3B), reflecting a ubiquitous presence at early stages of development. Later in embryogenesis and postnatally, expression became more restricted to highly proliferative tissues, such as the subventricular zone during neurogenesis and perinatal hair follicles (Figures S2C–S2F). In adults, RNase H2 was present in proliferative tissues, including intestinal crypt epithelium, and testes (Figures S2G and S2H). Expression correlated most closely with the proliferation marker Ki67, suggesting that RNase H2 is

(D) Multiplex PCR for mouse genotyping. (Top) A 221 bp PCR product (a→c) is present in wild-type mice (+/+); mice containing the *Rnaseh2b*^{E202X} allele (also) give a 460 bp product (a→b). (Bottom) Schematic indicating position of forward (a) and reverse primers (b and c).

(E) Mice with null mutations (m) in *Rnaseh2b* are not postnatally viable, whereas E6.5–E10.5 embryos are present at Mendelian ratios. Genotype frequencies for offspring at weaning (and for embryos at indicated stages) derived from *Rnaseh2b*$^{E202X/+}$ and *RNaseh2b*$^{tm1a/+}$ intercrosses respectively.

p values, χ^2 test; n.s., not significant; m, mutant allele. *Rnaseh2b* accession number: NM_026001.2.

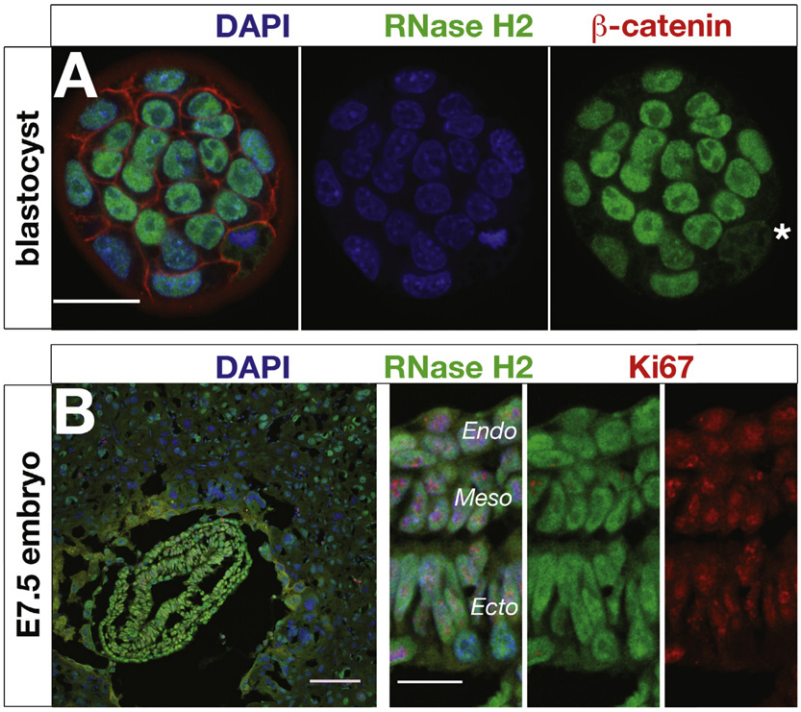

Figure 3. The RNase H2 Enzyme Is Expressed in Actively Proliferating Cells from Early Embryogenesis

(A) RNase H2 is expressed from early embryogenesis. Whole-mount immunostaining of wild-type mouse blastocysts detects endogenous RNase H2 expression in the nucleus of interphase cells and dispersed throughout the cell at mitosis (*). Scale bar, 20 μm.

(B) RNase H2 is expressed in all three cell layers of gastrulating mouse embryos. Confocal image of a wild-type cryosectioned E7.5 embryo, with Ki67 marking actively proliferating cells. Scale bar, 100 μm. (Insert) Higher-power view demonstrates strong nuclear localization in all three embryonic layers: endoderm (Endo), mesoderm (Meso), and ectoderm (Ecto). Scale bar, 20 μm. See also Figure S2.

preferentially expressed in actively cycling cells at all stages of the cell cycle. In support of this, western analysis from synchronized HeLa cells demonstrated uniform expression levels of all three RNase H2 subunits throughout the cell cycle (Figure S2I).

A p53-Dependent Damage Response Is Evident in RNaseH2^{null} Embryos

RNaseH2^{null} embryonic growth failure could be the consequence of inefficient DNA replication or activated DNA damage signaling. Embryonic tissues were therefore immunostained for histone H2A.X phosphorylated at serine 139 (pH2AX), a marker of DNA-damage response to double-strand breaks and arrested replication (Rogakou et al., 1998; Ward and Chen, 2001). Though no difference in pH2AX levels was observed between mutant and control blastocysts, at E6.5, there was a substantial increase in nuclear pH2AX staining in epiblast cells of RNaseH2^{null} embryos (Figure 4A), coinciding with a period of rapid cell cycles of less than 6 hr (Snow, 1977).

At E6.5, there was no alteration in the percentage of epiblast cells undergoing active DNA synthesis; however, by E7.5, a significant reduction was evident (Figures 4B and 4C). Reduced embryo growth appeared to be the result of arrested cell proliferation, rather than cell death, as no widespread increase in apoptosis was observed at E7.5 or E9.5 by activated caspase 3 immunostaining (data not shown).

To investigate the molecular basis of this growth arrest, whole-genome expression analysis was performed using Illumina microarrays. Transcript levels of 197 genes were significantly upregulated in E9.5 mutant embryos, whereas 115 genes were downregulated when compared to age-matched controls ($p < 0.05$; > 1.5-fold change). Of note, the four genes with the greatest fold increase in expression (Figure 4D), *Ccng1/Cyclin G1*, *Cdkn1a/p21*, *Phlda3*, and *Trp53inp1*, were all targets of the p53 transcriptional activator, a key transducer of ATM/ATR DNA damage signaling (Tibbetts et al., 1999; Yajima et al., 2006). Increased *Cyclin G1* and *p21* expression was confirmed by qPCR and immunoblotting (Figure 4E). In addition, *Rnaseh2b* was found to be <0.02% of wild-type by qPCR, in keeping with nonsense-mediated decay of this transcript (Figure 4E). Although RNase H2 could have a role in suppressing expression of endogenous retroelements (Bhoj and Chen, 2008), no changes in retroelement transcript levels were identified, indicating that there was no widespread dysregulation of retroelements at this stage of embryonic development. Similarly, there was no transcriptional evidence of an immune-mediated process (data not shown).

We postulated that the DNA damage observed in the E6.5 embryos led to p53 activation and reduced cellular proliferation as a consequence of cyclin G1 and p21-mediated cell-cycle arrest (Cazzalini et al., 2010; Kimura et al., 2001). In keeping with this, partial rescue of the RNaseH2^{null} embryonic phenotype was observed in a *p53*$^{-/-}$ background (Figure S3). Loss of p53 also fully rescued defective cell proliferation (Figure 4F) in primary cultures of E10.5/E11.5 mesodermal tissue, performed to generate mouse embryonic fibroblast (MEF) cell lines. *Rnaseh2b*$^{-/-}$;*p53*$^{+/+}$ cells completely failed to proliferate in culture (2/2), whereas those derived from *Rnaseh2b*$^{-/-}$;*p53*$^{-/-}$ embryos grew well ($p < 0.001$; 5/5), though at 64% of the rate of *Rnaseh2b*$^{+/+}$;*p53*$^{-/-}$ MEFs (Figures 4F and 4G). *Rnaseh2b*$^{-/-}$;*p53*$^{+/-}$ cells showed very limited growth, and though MEF cell lines were eventually established from three out of eight embryos, all were found to have then lost the remaining wild-type *p53* allele (data not shown). In conclusion, loss of RNase H2 enzyme activity results in p53-mediated arrest of cell growth.

Ribonucleotide Accumulation in Genomic DNA of RNaseH2^{null} Cells

Rnaseh2b$^{-/-}$;*p53*$^{-/-}$ MEFs were next used to investigate the molecular consequences of RNase H2 loss. As expected,

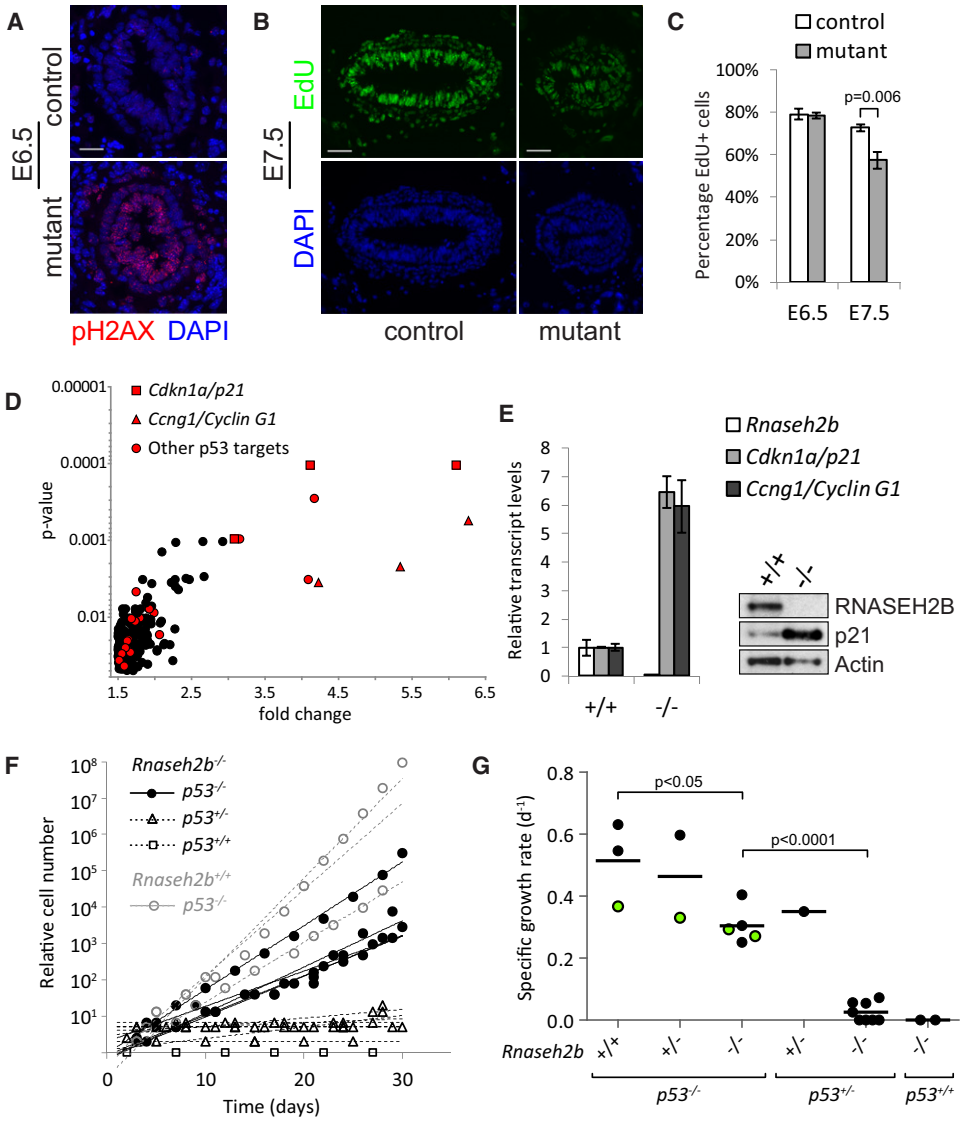

Figure 4. A p53-Dependent DNA-Damage Response Is Activated in RNase H2-Deficient Embryos, Leading to Arrest in Cellular Proliferation

(A) Markedly elevated levels of nuclear pH2AX foci are evident in the epiblast of E6.5 embryos. Confocal projection of transverse cryosections through the decidua of E6.5 mutant RNaseH2^{null} and control littermate embryos. Scale bar, 10 μm.

(B and C) The number of S phase epiblast cells is reduced in E7.5 embryos.

(B) Representative immunofluorescence confocal projections of 10 μm cryosections from E7.5 mutant and control embryos. Embryos fixed 1 hr after intraperitoneal injection of 100 mg/kg into pregnant females and EdU visualized by Click-iT (Invitrogen), counterstained with DAPI (blue). Scale bar, 50 μm.

(C) Relative proportions of EdU- incorporating cells in E6.5 and E7.5 embryos demonstrate a significant reduction at E7.5 in RNaseH2^{null} embryos (t test; n = 5 embryos per data point, >200 epiblast cells/embryo). S phase index determined from EdU-positive nuclei/total nuclei. Error bars represent SEM.

(D) Significant upregulation of p53 target genes in E9.5 RNaseH2^{null} embryos is detected by Illumina MouseWG-6 v2.0 Expression BeadChip microarray analysis. Plotted data points correspond to Illumina probes.

(E) qPCR confirms a 6-fold upregulation of *Cyclin G1* and *p21* transcripts in E9.5 mutant embryos (error bars represent SD of technical triplicates). Immunoblotting of total cell lysates from E9.5 mutant embryos demonstrates increased p21 protein levels. Loading control, actin.

(F and G) Cell-cycle arrest in RNaseH2^{null} embryos is p53 dependent.

(F) Growth kinetics from primary culture of mesenchymal cells recovered from E10.5 and E11.5 RNaseH2^{null} embryos show that RNaseH2^{null} cells from *p53*$^{-/-}$ (n = 5), but not *p53*$^{+/-}$ (n = 8) and *p53*$^{+/+}$ (n = 2), littermates are capable of proliferation. Growth curves for *Rnase2b*$^{+/+}$;*p53*$^{-/-}$ cells (n = 3) derived from littermates are shown for comparison.

(G) Specific growth rates of MEFs calculated from growth kinetics as shown in (F). *Rnase2b*$^{-/-}$;p53$^{-/-}$ cells initially grew with doubling times of 2.4 ± 0.4 days compared with *Rnase2b*$^{+/+}$;p53$^{-/-}$ cells that doubled every 1.5 ± 0.5 days ($p < 0.05$). This difference became negligible at later passages (data not shown). Green circles correspond to MEF lines used for further analysis.

See also Figure S3.

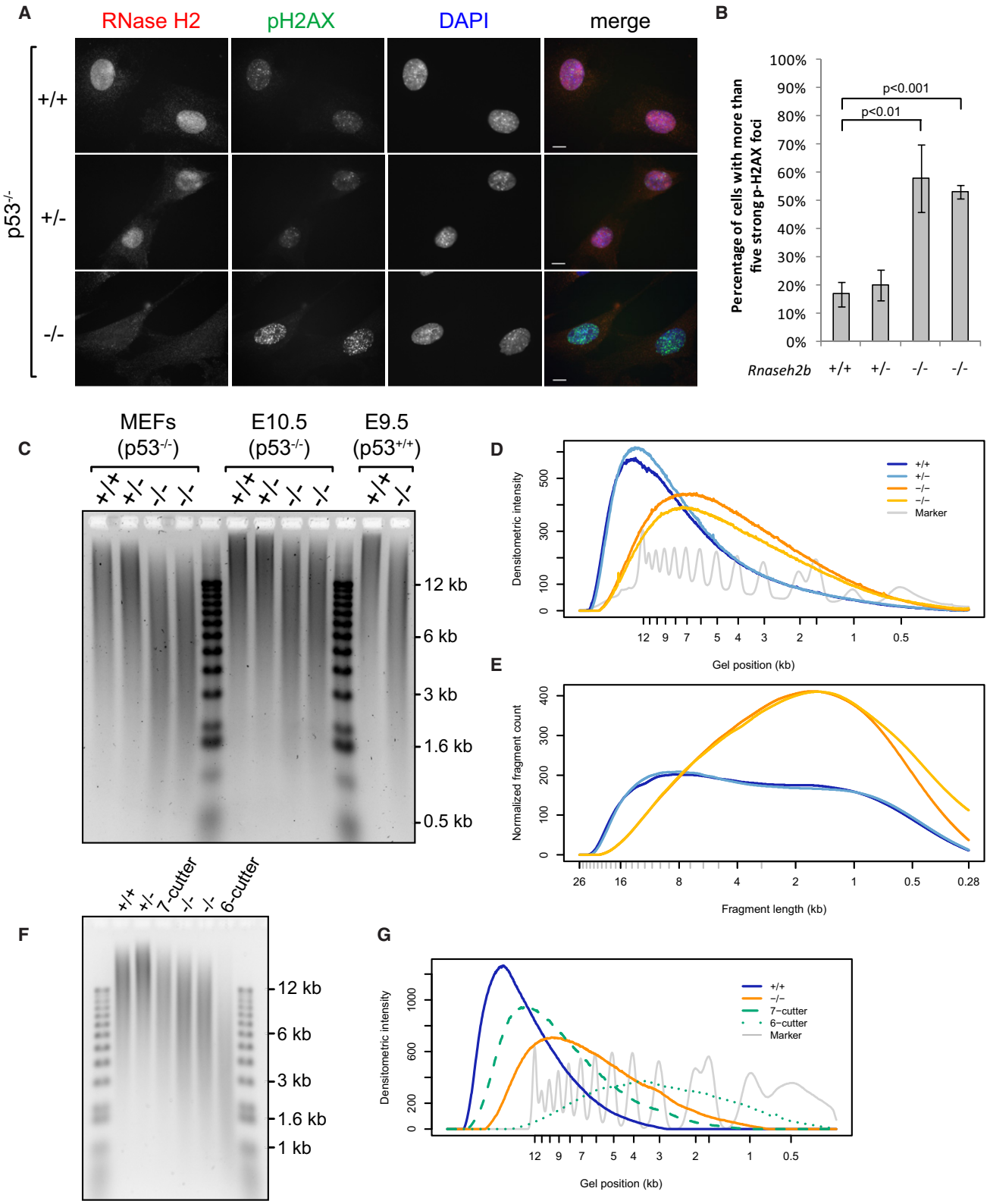

Figure 5. RNaseH2^{null} Genomic DNA Is More Sensitive to Alkali Hydrolysis

(A and B) Levels of pH2AX foci are elevated in *Rnase2b*$^{-/-}$;*p53*$^{-/-}$ MEFs.

(A) Representative immunofluorescent images of *Rnaseh2b*$^{+/+}$, $^{+/-}$, $^{-/-}$ cell lines. Scale bar, 10 μm.

type 2 RNase H activity and the RNase H2 protein complex were absent in these cell lines (Figures S4A and S4B). Significantly elevated levels of pH2AX foci were also present (Figures 5A and 5B), indicative of DNA double-strand breaks and/or replication fork arrest. In addition, we examined polyADPribosylation (PAR) as another early marker of DNA-damage activation, which occurs in response to DNA breaks (Caldecott, 2008; Satoh and Lindahl, 1992). Levels of PAR were substantially raised in RNaseH2^{null} MEFs, as shown by immunoblotting (Figure S4C), confirming the presence of cellular DNA-strand breaks.

DNA damage in RNaseH2^{null} cells might arise as the consequence of undegraded Okazaki RNA primers, misincorporation of ribonucleotides by DNA polymerases, or transcriptionally induced R loops. To discriminate between these possibilities, total nucleic acids from the MEFs were separated by gel electrophoresis under alkaline conditions. Substantially increased mobility of genomic DNA from both RNaseH2^{null} cell lines after treatment with alkali was observed relative to control genomic DNA (Figures 5C–5E), whereas no significant difference was evident upon electrophoresis under neutral conditions (Figure S4D). Given that phosphodiester bonds 3′ of ribonucleotides, but not deoxynucleotides, are sensitive to alkali hydrolysis through nucleophilic attack by the 2′ hydroxyl group (Lipkin et al., 1954), such increased fragmentation (termed alkali sensitivity) likely indicates the incorporation of ribonucleotides into genomic DNA. Given that alkali treatment also denatures DNA, increased electrophoretic mobility could also be the consequence of increased nicking, or gaps, in genomic DNA. To address this possibility, gel electrophoresis of total cellular nucleic acids was performed after formamide denaturation, which denatures DNA (Tang et al., 1989) without hydrolyzing ribonucleotide phosphodiester bonds (Figure 6A). Under these conditions, RNaseH2^{null} DNA did not demonstrate increased mobility, in contrast to DNA treated with Nt.*Bsp*QI nicking endonuclease, which on average introduces nicks every ~11 kb. Therefore, the observed alkali-sensitive sites were consistent with covalently incorporated ribonucleotides, rather than gaps or nicks in genomic DNA.

Treatment with recombinant RNase H2 enzyme also led to widespread fragmentation of RNaseH2^{null} genomic DNA, as shown by increased electrophoretic mobility after formamide denaturation. Significantly, the resulting fragmentation pattern was essentially identical to that seen after alkali treatment (Figure 6B), whereas no increased mobility was observed when inactive recombinant RNase H2 was used. In distinct contrast, recombinant *E. coli* type-1 RNase H (RNase HI) had no visible impact on the mobility of RNaseH2^{null} genomic DNA (Figure 6C). RNase HI efficiently digests substrates with four or more ribonucleotides but can also hydrolyze double-stranded nucleic acids with three embedded ribonucleotides, albeit at substantially lower rates (Hogrefe et al., 1990). Although the biological significance of this activity is unclear, oligonucleotide substrates with three ribonucleotides were cleaved efficiently under our assay conditions (Figures S5C and S5D). This activity was fully preserved in the presence of RNaseH2^{null} genomic DNA, ruling out any inhibitory effects that may be present within the nucleic acid preparation (Figures S5A–S5C). Thus, the differential sensitivity of genomic DNA from RNaseH2^{null} cells to RNase HI and RNase H2 activities established that the alkali and RNase H2 cleavable sites consist of one or, at most, two consecutive covalently incorporated ribonucleotides.

Quantitative analysis of the alkali-induced fragmentation permitted us to estimate the frequency of embedded ribonucleotides. Determination of DNA fragment distributions (Figure 5E) from the densitometry data (Figure 5D) predicted a rate of ribonucleotide incorporation of ~1 in 7,600 nucleotides (nt) (analytical method described in Figure S4F). Additionally, the fragmentation pattern of hydrolyzed RNaseH2^{null} DNA lies between that generated by two nicking endonucleases, one that cuts, on average, once every 11 kb (7-cutter Nt.*Bsp*QI) and the other once every 3.7 kb (6-cutter Nb.*Bts*I) in the mouse reference genome (Figures 5F and 5G), supporting the computational estimate. Early and late passage MEFs exhibited similar levels of alkali sensitivity (data not shown). The incorporation of 1 ribonucleotide every 7,600 nucleotides during each round of replication would maintain such a steady-state level, so this is a minimum estimate for in vivo ribonucleotide misincorporation by polymerases.

Taken together, these results demonstrate the widespread presence of incorporated ribonucleotides in genomic DNA of RNaseH2^{null} MEFs. Ribonucleotide misincorporation was also evident in RNaseH2^{null} embryos (Figures 5C and S4E), consistent with this molecular defect underlying the developmental

(B) Quantification for (A). Cells with five or more strong pH2AX foci. Error bars represent SD. n = 3 expts, > 100 cells/expt, t test. From here on +/+, +/−, −/−, and −/− indicate *Rnaseh2b* genotypes of four independent MEF lines.

(C and D) Genomic DNA from RNaseH2^{null} cells display markedly increased alkali sensitivity.

(C) Representative gel of total nucleic acids from *Rnaseh2b*$^{+/+}$, $^{+/-}$, $^{-/-}$ MEFs and yolk sacs separated by alkaline agarose gel electrophoresis after alkaline hydrolysis.

(D) Densitometry of the first five lanes of (C), plotted using Aida 2D densitometry software, demonstrates a substantial shift in migration of RNaseH2^{null} MEF genomic DNA fragments.

(E) Quantification of DNA fragmentation pattern calculated from densitometry traces shown in (D). Densitometry intensity distribution is divided by the fragment length distribution to quantitate the proportion of molecules of a particular fragment size. Fragment counts are normalized so that total nucleotide number is equal between samples.

(F and G) Alkali treatment fragments RNaseH2^{null} DNA to an average size that lies between 3.7 and 11 kb.

(F) Fragmentation pattern of RNaseH2^{null} (−/−) alkali-treated DNA compared with that of the nicking endonucleases Nt.*Bsp*QI, which cuts mouse genomic DNA on average every 11 kb (7-cutter), and Nb.*Bts*I, which cuts on average every 3.7 kb (6-cutter).

(G) Densitometry of selected lanes from (F).

See also Figure S4.

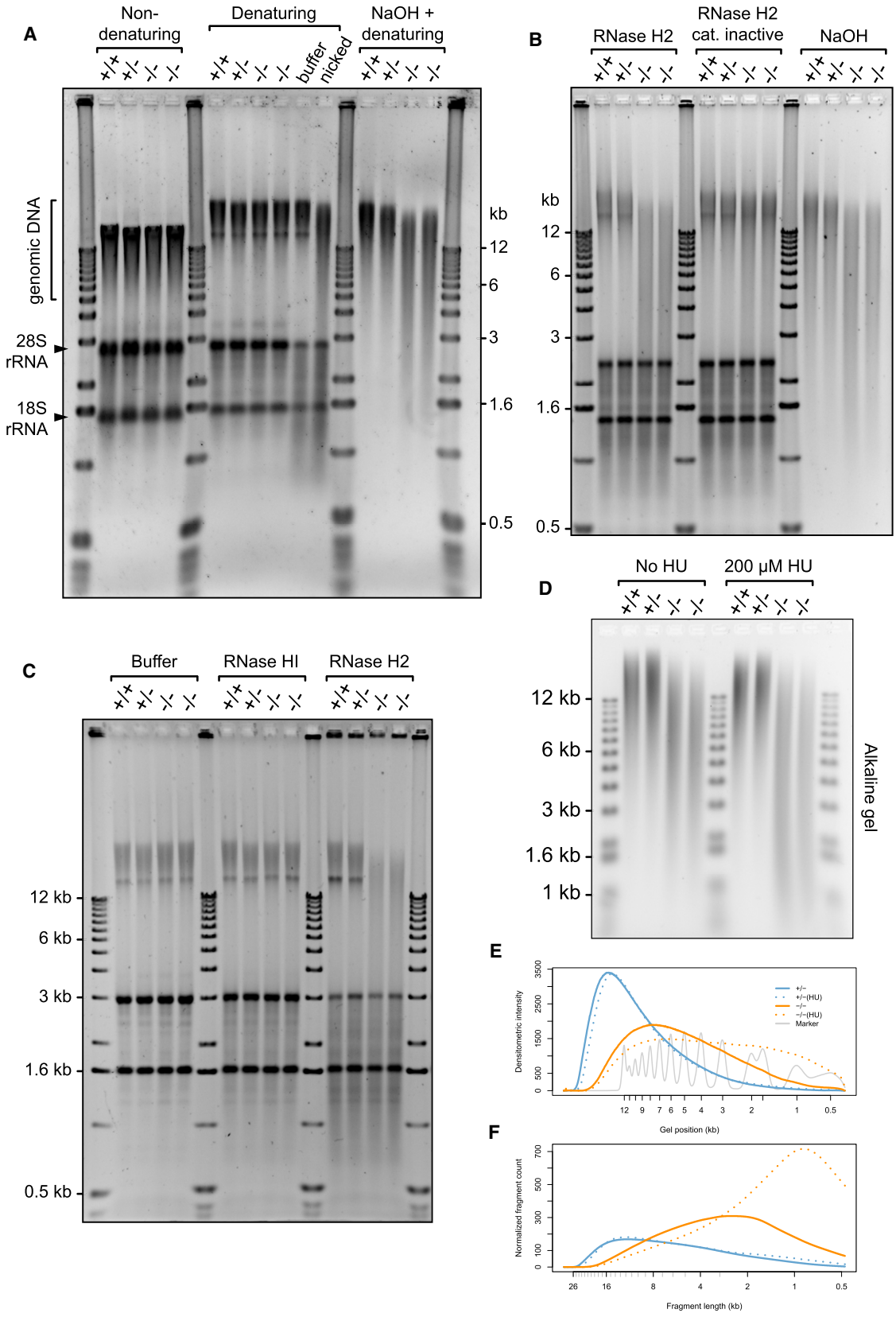
A
Non-denaturing
Denaturing
NaOH + denaturing
+/+
+/-
-/-
-/-
buffer
nicked
genomic DNA
28S rRNA
18S rRNA
kb
12
6
3
1.6
0.5
B
RNase H2
RNase H2 cat. inactive
NaOH
kb
12
6
3
1.6
0.5
C
Buffer
RNase HI
RNase H2
12 kb
6 kb
3 kb
1.6 kb
0.5 kb
D
No HU
200 μM HU
12 kb
6 kb
3 kb
1.6 kb
1 kb
Alkaline gel
E
Densitometric intensity
+/-
+/-(HU)
-/-
-/-(HU)
Marker
Gel position (kb)
F
Normalized fragment count
Fragment length (kb)

phenotype. Finally, we employed a chemical genetic approach analogous to previous yeast genetic experiments, in which a mutated Pol ε with an enhanced propensity for ribonucleotide incorporation was used (Nick McElhinny et al., 2010b). Cells were treated with a low dose of hydroxyurea (HU) to reduce cellular dNTP:rNTP ratios through partial inhibition of ribonucleotide reductase activity. This would then increase ribonucleotide incorporation by DNA polymerases. RNaseH2^{null} cells were observed to be hypersensitive to such a low dose of HU, accumulating in S phase (Figure S5G). Most significantly, such treatment resulted in additional alkali and RNase H2-sensitive sites in genomic DNA from RNaseH2^{null} cells (Figures 6D–6F, S5E, and S5F), consistent with such sites resulting from ribonucleotide misincorporation by DNA polymerases.

Chromosome Instability in RNaseH2^{null} Cells

Substantial levels of micronuclei, indicative of chromosomal breakage (Norppa and Falck, 2003), were observed in RNaseH2^{null} MEFs (Figure 7A), suggesting that the excessive presence of ribonucleotides in DNA causes large-scale genome instability. Likewise, large-scale cytogenetic anomalies were evident in DAPI-stained metaphase chromosomes (Figure 7B). Using satellite FISH probes, chromosomal rearrangements were present in virtually all metaphases from *Rnaseh2b*$^{-/-}$;*p53*$^{-/-}$ MEFs, whereas they were only occasionally seen in control MEFs. Both minutes (marker chromosomes) and interchromosomal translocations were frequently observed, with translocations confirmed by FISH and chromosomal painting (Figures 7, S6A, and S6B).

DISCUSSION

Ribonucleotides Accumulate in RNaseH2^{null} Cells as a Consequence of Incorporation by DNA Polymerases

Here, we report that substantial genome-wide incorporation of ribonucleotides occurs in mammalian genomic DNA and establish that RNase H2 is required for efficient removal of such nucleotides. Recent in vitro biochemical studies with yeast replicative polymerases have shown the misincorporation of ribonucleotides into DNA (Nick McElhinny et al., 2010a). Based on these findings, it was predicted that ribonucleotides may be incorporated into genomic DNA in vivo. Subsequent studies in both fission and budding yeast have established that this is indeed the case using alkali sensitivity assays of yeast genomic DNA (Miyabe et al., 2011; Nick McElhinny et al., 2010b). Here, we show that ribonucleotide incorporation also occurs in metazoans; demonstrate that such ribonucleotide lesions are harmful to mammalian cells; and establish that their removal is required for mouse embryonic development. Previous studies used an elegant genetic approach in which mutator replicative polymerases with increased propensity for ribonucleotide incorporation were used to infer the presence of incorporated ribonucleotides from enhanced alkali sensitivity of RNase H2 null yeast genomic DNA. Our findings provide further characterization of these alkali-sensitive sites by using enzymatic assays to directly substantiate that such lesions are single or diribonucleotides that are covalently incorporated into genomic DNA. Furthermore, we find that such lesions occur at a frequency of least 1,000,000 sites per cell, establishing them as the most common endogenous base lesions in the mammalian genome.

The presence of such ribonucleotides is most readily explained by misincorporation by the major replicative polymerases, which are estimated to incorporate one ribonucleotide every few thousand nucleotides in vitro (Nick McElhinny et al., 2010a). Alternatively, embedded ribonucleotides could result from failure to remove RNA primers during Okazaki-lagging strand processing. Such primers are ~10 nt in length, much longer than the single/diribonucleotides found. However, retention of single ribonucleotides during this process remains a possibility (Rumbaugh et al., 1997). Theoretically, oxidation of deoxynucleotides that are present in DNA could also result in embedded ribonucleotides (Vengrova and Dalgaard, 2004), although this seems an unlikely explanation for their frequent occurrence.

Genomic DNA from RNase H2 null *S. cerevisiae* exhibits differential alkali sensitivity that correlates with the propensity of a mutant Pol ε to incorporate ribonucleotides (Nick McElhinny et al., 2010b). Here, we performed an analogous experiment using hydroxyurea to alter dNTP:rNTP ratios, favoring ribonucleotide incorporation. This promoted increased alkali and RNase H2 sensitivity, leading us to conclude that ribonucleotides that are embedded in genomic DNA are most likely the consequence of misincorporation by DNA polymerases. Given their frequent occurrence in genomic DNA, the predominant sources of such ribonucleotides are likely to be Pol ε and Pol δ, the major replicative polymerases that are responsible for leading- and lagging-strand synthesis, respectively (Burgers, 2009; Kunkel and

Figure 6. Covalently Incorporated Ribonucleotides Are Present in Nuclear DNA of RNaseH2^{null} Cells

(A–C) *Rnase2b*$^{-/-}$;*p53*$^{-/-}$ genomic DNA contains mono or diribonucleotides. Total nucleic acids isolated from *p53*$^{-/-}$ MEFs were separated by agarose gel electrophoresis under native conditions or after denaturation with 90% formamide.

(A) Genomic DNA from RNaseH2^{null} cells does not contain elevated numbers of nicks. Increased nicking is detected only in genomic DNA treated with Nt.*Bsp*QI nicking endonuclease. (+/+, +/−, −/−,−/−) *Rnaseh2b* genotypes of four independent MEF lines.

(B) RNase H2 fragments genomic DNA from RNaseH2^{null} cells to the same extent as hydrolysis with NaOH. Total nucleic acids isolated from passage matched *p53*$^{-/-}$ MEFs ± *Rnaseh2b* treated with purified recombinant human RNase H2, catalytically inactive RNase H2 (RNASEH2A-D34A/D169A), or NaOH and were then denatured with 90% formamide.

(C) Recombinant RNase HI, which cleaves DNA duplexes with three or more embedded ribonucleotides, does not fragment DNA from RNaseH2^{null} MEFs. Treated nucleic acids were denatured with 90% formamide.

(D–F) RNaseH2^{null} cells have increased ribonucleotide incorporation, reflected by enhanced alkali sensitivity after low-dose hydroxyurea treatment. Alkali gel electrophoresis of total nucleic acids from four independent MEF cell lines with and without hydroxyuea (HU) treatment (200 μM for 48 hr). (E) Densitometry traces of selected lanes from (D) as indicated and (F) quantification of fragmentation pattern.

See also Figure S5.

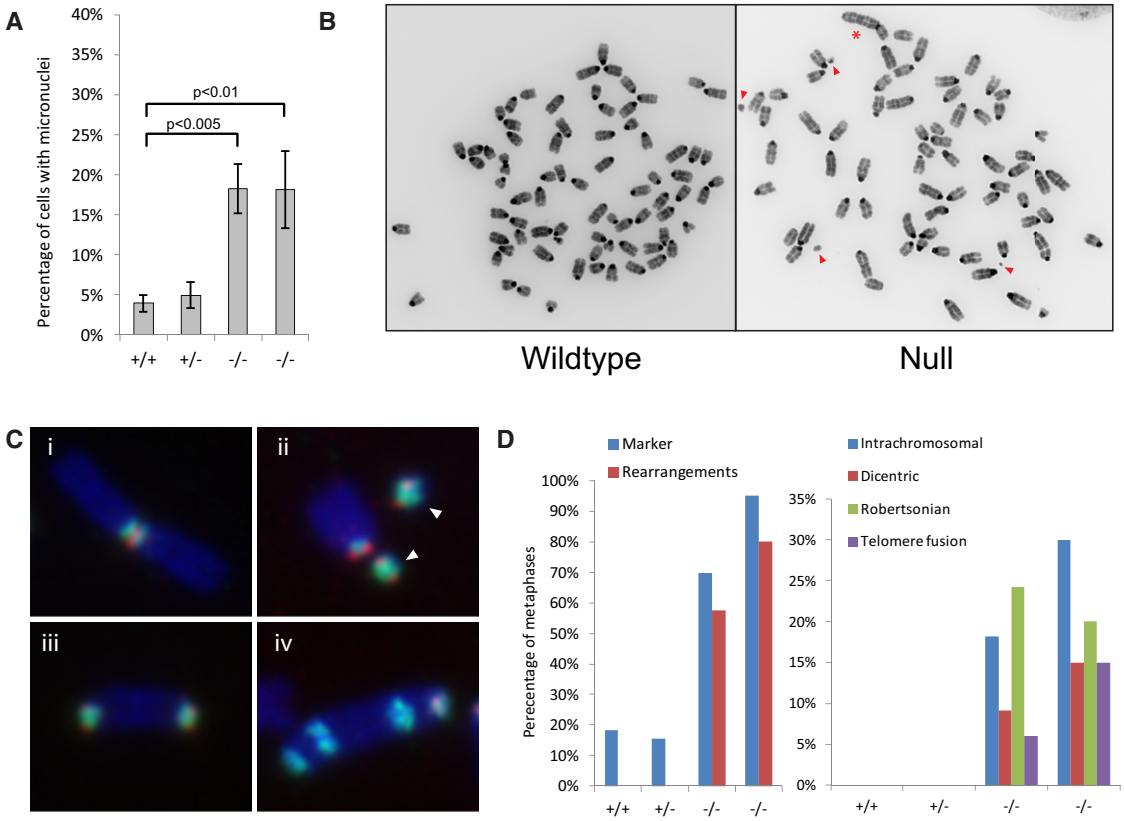

Figure 7. RNaseH2^{null} Cells Display Large-Scale Genome Instability

(A) Micronuclei are frequently present in *Rnase2b*$^{-/-}$;*p53*$^{-/-}$ cells. Error bars represent SD. n = 3 expts 500–1000 cells/expt. p value, t test.

(B) Chromosomal rearrangements (asterisk) and marker chromosomes (arrowheads) are evident in DAPI-stained metaphase chromosomes of *Rnase2b*$^{-/-}$;*p53*$^{-/-}$ MEFs.

(C and D) FISH for major (green) and minor (red) satellite probes confirms the presence of frequent intrachromosomal translocations and heterochromatic minutes (marker chromosomes). (i) Robertsonian translocation, (ii) heterochromatic marker chromosomes (arrowheads), (iii) end-to-end translocation, and (iv) complex chromosomal rearrangement. (D) Quantification of cytogenetic anomalies identified in (C). n = 38, 32, 33, and 20 metaphases, respectively. $p < 0.05$ (Fisher's exact test) for all wild-type (+/+) versus mutant (−/−) comparisons.

See also Figure S6.

Burgers, 2008; Miyabe et al., 2011). However, other DNA polymerases, such as Pol β (Cavanaugh et al., 2010) and lesion bypass polymerases, may also contribute.

RNase H2 Is a Genome Surveillance Enzyme Required for Ribonucleotide Removal

Ribonucleotide accumulation in genomic DNA of RNaseH2^{null} mice (Figures 5 and 6) implicates the RNase H2 complex in the maintenance of genome integrity. This DNA repair function was originally suggested by Eder and colleagues (Eder et al., 1993). Ribonucleotides are likely to be harmful, as their ribose 2′-hydroxyl group increases susceptibility of the adjacent phosphodiester bond to hydrolysis. Specific patterns of mutations at nucleotide level have been observed in genomic DNA from RNase H2 null *S. cerevisiae* (Kim et al., 2011; Nick McElhinny et al., 2010a). Most frequently, these consist of 2–5 bp deletions, which are the result of topoisomerase-I-induced nicks at embedded ribonucleotides (Kim et al., 2011). However, the loss of yeast RNase H2 alone has a relatively small effect on mutation frequency, and the effect of embedded ribonucleotides on large-scale genome stability in yeast has not been reported. Therefore, the frequent occurrence of large-scale genome rearrangements in RNaseH2^{null} MEFs is unanticipated and noteworthy (Figure 7).

We estimate that ribonucleotides are incorporated at a rate of at least 1 every 7,600 nt in RNaseH2^{null} cells, corresponding to ~1,300,000 lesions per cell. This is within the same order of magnitude predicted from in vitro incorporation rates by eukaryotic replicative polymerases (Nick McElhinny et al., 2010a) and is substantially higher than any other endogenous base lesions occurring in the mammalian genome. Even the previously most common lesions, such as abasic sites, 8-hydroxyguanine (8-oxoG), and 7-methylguanine, only occur up to 10,000 times per genome (Ciccia and Elledge, 2010; Lindahl and Barnes, 2000). As misincorporated ribonucleotides occur at at least 50-fold higher rates, without an efficient repair mechanism, they would be the most common noncanonical nucleotides present in mammalian DNA. Therefore, defining the processes that remove these ribonucleotides is of substantial interest. Of note, FEN1/Rad27 in conjunction with RNase H2 can excise

ribonucleotides on an in vitro substrate, generating a single nucleotide gap on which a DNA polymerase and DNA ligase could act directly to repair the lesion (Rydberg and Game, 2002).

Misincorporated Ribonucleotides Induce DNA Damage

In itself, ribonucleotide incorporation does not prevent replication: cellular proliferation is seen in both RNase H2 null mouse cells ($p53^{-/-}$; Figure 4) and RNase H2 null budding yeast, in which p53 signaling is not evolutionarily conserved (Arudchandran et al., 2000; Belyi et al., 2010; Nick McElhinny et al., 2010b). DNA polymerases can tolerate templates containing ribonucleotides (Watt et al., 2011), which may explain why early embryogenesis in $RNaseH2^{null}$ embryos proceeds normally. The absence of grossly perturbed transcriptional profiles later in development (Figure 4) suggests that mammalian RNA polymerases also tolerate ribonucleotide-containing templates.

However, excessive numbers of ribonucleotides do appear to be problematic. Replication fork stalling may occur in regions that contain clustered ribonucleotides, as seen at the *S. pombe* mating switch locus (Vengrova and Dalgaard, 2006). Incorporation of ribonucleotides in difficult to replicate regions or in close proximity to other lesions may be similarly detrimental. This is likely to explain the activation of DNA-damage response signaling observed in $RNaseH2^{null}$ MEFs and embryos (Figures 4 and 5). Chromosomal rearrangements and micronuclei indicate the occurrence of double-strand DNA breaks. Such breaks may result from subsequent replication fork collapse or may be caused directly by hydrolysis of ribonucleotides on opposing DNA strands (see model in Figures S6C and S6D). Alternatively, the observed increase in PAR (Figure S4C) could suggest the presence of frequent single-strand breaks that would be converted at low frequency to double-strand lesions during replication. The accumulation of ribonucleotides in conjunction with rapid cell cycles in the epiblast (Snow, 1977) probably underlies the marked activation of DNA-damage signaling in the embryo. This then results in a p53-mediated inhibition of proliferation that is likely to substantially contribute to the lethality observed at E11.5 in $RNaseH2^{null}$ embryos.

Ribonucleotide Incorporation in Health and Disease

To our knowledge, stable incorporation of ribonucleotides has only been reported to date in two contexts. First, a diribonucleotide at the *S. pombe* mating switch locus is believed to be the signal initiating homologous recombination (Vengrova and Dalgaard, 2004). Second, the presence of ribonucleotides in mature mitochondrial DNA has been previously established (Grossman et al., 1973), and we now show these to be mono or diribonucleotides (Figure S5H). These sporadic ribonucleotides appear to be randomly distributed and thus are likely to result from replicative polymerase incorporation. The selectivity of the mitochondrial polymerase γ would be consistent with the presence of 10–30 ribonucleotides in mature mtDNA (Kasiviswanathan and Copeland, 2011). These may be tolerated by the mitochondrial genome either because of its relatively slow replication rate (Bogenhagen and Clayton, 1977) or owing to different mechanism(s) of genome replication (Clayton, 2003; Holt, 2009). Likewise, ribonucleotide incorporation is well tolerated in RNase H2-deficient *S. cerevisiae*, with normal viability and efficient cellular proliferation in unperturbed cells (Arudchandran et al., 2000; Nick McElhinny et al., 2010b). As recently reported, template switch and translesion DNA synthesis postreplication repair pathways may permit such ribonucleotides to be tolerated (Lazzaro et al., 2012). In contrast, in mice, we find that ribonucleotide removal is essential early in development. Similarly, mutation of other genes ensuring genome integrity, such as the catalytic subunit of pol ζ (Rev3), are viable in yeast but cause embryonic lethality at a similar stage in mutant mice (Esposito et al., 2000; Wittschieben et al., 2000). Such lethality may therefore be explained by the much larger size and complexity of the mammalian nuclear genome.

Low levels of ribonucleotide incorporation in the nuclear genome may be tolerated, and this could well be relevant to the autoinflammatory disorder Aicardi-Goutières syndrome (AGS), in which aberrant nucleic acid substrates are thought to drive an innate immune response (Crow and Rehwinkel, 2009). Reduced RNase H2 activity in AGS may therefore result in a chronic low level of ribonucleotide incorporation that is then processed by alternative (non-RNase H2 dependent) repair pathways. The increased levels of polyADPribosylation (Figure S4C), as well as the enhanced sensitivity to hydroxyurea observed in $Rnaseh2b^{+/-}$ MEFs (Figure S5G), could be consistent with this possibility. Aberrant nucleic acid species generated by such repair could then trigger an innate immune response. Alternatively, embedded ribonucleotides might induce DNA-damage response signaling that itself stimulates interferon production (Brzostek-Racine et al., 2011).

In summary, ribonucleotides are highly deleterious to the mammalian cell when left incorporated in the nuclear genome, causing substantial genome instability. RNase H2 is therefore a critical enzyme for ensuring the integrity of genomic DNA. Defining the pathway(s) that remove these ribonucleotides from genomic DNA, the site and nature of ribonucleotide-induced DNA damage, as well as the genome distribution of ribonucleotides will now be of substantial interest. This will help improve our understanding of the pathological and physiological roles of ribonucleotides in genomic DNA, of significance to both nucleic acid-driven autoimmunity and carcinogenesis.

EXPERIMENTAL PROCEDURES

Generation of *Rnaseh2b* Null Mice

While performing targeted homologous recombination to generate 129/Ola ES cells with a c.520G > A (A174T) mutation in exon 7 of *Rnaseh2b* (that corresponds to the most common, hypomorphic AGS patient mutation, c.529G > A), we identified the $Rnaseh2b^{E202X}$ ES clone that had fortuitously acquired an additional mutation resulting in a premature stop codon: c.604G > T, E202X. Further details of gene targeting are available in the Supplemental Information. After karyotyping and blastocyst injection, resulting male chimeras were crossed to C57BL/6J females, giving rise to heterozygous *Rnaseh2b* knockin mice carrying both A174T and E202X mutations ($Rnaseh2b^{tm1\text{-}hgu\text{-}A174T,E202X}$, elsewhere referred to as $Rnaseh2b^{E202X}$). Crosses with $p53^{+/-}$ mice (Clarke et al., 1993) were used to generate $Rnaseh2b^{E202X/+};p53^{+/-}$ double mutants. Knockout-first *Rnaseh2b* mice were generated by blastocyst injection of the $Rnaseh2b^{tm1a(EUCOMM)Wtsi}$ ES cell clone EPD0087_4_A02 (EUCOMM ID: 24441; elsewhere referred to as $Rnaseh2b^{tm1a}$) (Friedel et al., 2007). The $Rnaseh2b^{tm1a}$ allele is designed to prematurely truncate *Rnaseh2b* transcripts through targeted insertion into

intron 4 of a genetrap cassette that contains a strong splice acceptor and an efficient polyadenylation signal (Testa et al., 2004).

Genotyping

Genotypes of mice and embryos were determined by multiplex PCR. The status of early embryos was determined by α-RNase H2 immunofluorescence. For further details and primer sequences, see Supplemental Information and Table S1.

RNase H Activity Assays

Enzyme activity assays were performed in triplicate using a FRET-based fluorescent substrate release assay as previously described (Crow et al., 2006a; Reijns et al., 2011) using 100 ng/μl of total protein from whole-cell extracts. RNase H2-specific activity was determined by subtracting the cellular activity against a sequence-matched DNA duplex without ribonucleotides.

Western Blotting, Immunohistochemistry, Immunocytochemistry, and Microscopy

Immunoblotting was performed on whole-cell extracts as described previously (Crow et al., 2006a). For immunohistochemistry, tissues and deciduas were dissected into ice-cold PBS and fixed with 4% paraformaldehyde/PBS for 3–16 hr at 4°C with further processing performed by standard methods. Images were collected on Zeiss Axioplan II fluorescence or Nikon A1R confocal microscopes. For full experimental details, see the Supplemental Information; for antibodies and dilutions, see Table S2.

Detection of Ribonucleotides in Genomic DNA

Total nucleic acids were isolated by mechanical disruption of MEFs or yolk sacks in ice-cold lysis buffer (20 mM Tris-HCl [pH 7.5], 75 mM NaCl, and 50 mM EDTA) and subsequent incubation with 100 μg/ml proteinase K, with Sarcosine then added to final 1% concentration. Nucleic acids were sequentially extracted with TE-equilibrated phenol, phenol:chloroform:isoamylalcohol (25:24:1), and chloroform; precipitated with isopropanol; washed with 75% ethanol; and dissolved in water. Mitochondrial DNA (mtDNA) was isolated from sucrose-gradient purified mitochondria as previously described (Pohjoismäki et al., 2010). For alkaline gel electrophoresis, total nucleic acids were heated for 2 hr at 55°C with 0.3 M NaOH and separated on agarose gels (50 mM NaOH, 1 mM EDTA) as previously described (Nick McElhinny et al., 2010b). Control samples were heated with 0.3 M NaCl and separated on 0.5× TBE agarose gels. Alternatively, nucleic acids were treated with RNase H enzymes and heated for 30–60 min in 90% formamide/20 mM EDTA at 37°C before separation on 0.5× TBE agarose gels. Digestions with RNase HI were carried out in 100 μl of 1× reaction buffer (NEB) with 5 U of enzyme for 1 hr at 37°C. Digestions with RNase H2 were carried out for 1 hr at 37°C in 100 μl reaction buffer (50 mM Tris [pH 8], 60 mM KCl, 10 mM $MgCl_2$, 0.01% BSA, 0.01% Triton) using 10 nM of purified recombinant human RNase H2 (Reijns et al., 2011). Nucleic acids were ethanol precipitated and dissolved in 90% formamide/20 mM EDTA. After electrophoresis, gels were stained with SYBR Gold (Invitrogen) or ethidium bromide.

ACCESSION NUMBERS

Microarray data for E9.5 *Rnaseh2b*$^{E202X/E202X}$ and wild-type embryos have been deposited in the Gene Expression Omnibus under the accession number GSE37419.

SUPPLEMENTAL INFORMATION

Supplemental Information includes Extended Experimental Procedures, six figures, and two tables and can be found with this article online at doi:10.1016/j.cell.2012.04.011.

ACKNOWLEDGMENTS

We thank I. Adams, N. Gilbert, N. Hastie, and I. Jackson for commenting on the manuscript; W. Bickmore, M. Ansari, D. Fitzpatrick, and T. Kunkel for helpful discussions; A. Ross, G. Waugh, J. Young, A. Hart, and C.A. Martin for technical assistance; A. Pearce, E. Maher, and E. Freyer for assistance with cytogenetic and FACS analysis; and C. Graham for statistical advice. We also thank Aurelio Reyes and Stuart Wood for providing mouse mitochondrial DNA and the Wellcome Trust Clinical Research Facility, Edinburgh for performing microarrays. This work was supported by funding from the MRC and Lister Institute for Preventative Medicine. A.P.J. is a MRC Senior Clinical Fellow and Lister Institute Prize Fellow.

Received: November 9, 2011
Revised: February 21, 2012
Accepted: April 23, 2012
Published online: May 10, 2012

REFERENCES

Alberts, B., Johnson, A., Lewis, J., Raff, M., Roberts, K., and Walter, P. (2002). Molecular biology of the Cell ((New York: Garland Science Taylor & Francis Group).

Arudchandran, A., Cerritelli, S., Narimatsu, S., Itaya, M., Shin, D.Y., Shimada, Y., and Crouch, R.J. (2000). The absence of ribonuclease H1 or H2 alters the sensitivity of Saccharomyces cerevisiae to hydroxyurea, caffeine and ethyl methanesulphonate: implications for roles of RNases H in DNA replication and repair. Genes Cells *5*, 789–802.

Belyi, V.A., Ak, P., Markert, E., Wang, H., Hu, W., Puzio-Kuter, A., and Levine, A.J. (2010). The origins and evolution of the p53 family of genes. Cold Spring Harb. Perspect. Biol. *2*, a001198.

Bhoj, V.G., and Chen, Z.J. (2008). Linking retroelements to autoimmunity. Cell *134*, 569–571.

Bogenhagen, D., and Clayton, D.A. (1977). Mouse L cell mitochondrial DNA molecules are selected randomly for replication throughout the cell cycle. Cell *11*, 719–727.

Brzostek-Racine, S., Gordon, C., Van Scoy, S., and Reich, N.C. (2011). The DNA damage response induces IFN. J. Immunol. *187*, 5336–5345.

Bubeck, D., Reijns, M.A., Graham, S.C., Astell, K.R., Jones, E.Y., and Jackson, A.P. (2011). PCNA directs type 2 RNase H activity on DNA replication and repair substrates. Nucleic Acids Res. *39*, 3652–3666.

Burgers, P.M. (2009). Polymerase dynamics at the eukaryotic DNA replication fork. J. Biol. Chem. *284*, 4041–4045.

Büsen. (1980). Purification, subunit structure, and serologicai analysis of calf thymus ribonuclease H I. J. Biol. Chem. *255*, 9434–9443.

Caldecott, K.W. (2008). Single-strand break repair and genetic disease. Nat. Rev. Genet. *9*, 619–631.

Cavanaugh, N.A., Beard, W.A., and Wilson, S.H. (2010). DNA polymerase beta ribonucleotide discrimination: insertion, misinsertion, extension, and coding. J. Biol. Chem. *285*, 24457–24465.

Cazzalini, O., Scovassi, A.I., Savio, M., Stivala, L.A., and Prosperi, E. (2010). Multiple roles of the cell cycle inhibitor p21CDKN1A in the DNA damage response. Mutat. Res. *704*, 12–20.

Cech, T.R. (2011). The RNA Worlds in Context. Cold Spring Harb. Perspect. Biol.

Cerritelli, S.M., and Crouch, R.J. (2009). Ribonuclease H: the enzymes in eukaryotes. FEBS J. *276*, 1494–1505.

Cerritelli, S.M., Frolova, E.G., Feng, C., Grinberg, A., Love, P.E., and Crouch, R.J. (2003). Failure to produce mitochondrial DNA results in embryonic lethality in Rnaseh1 null mice. Mol. Cell *11*, 807–815.

Chon, H., Vassilev, A., DePamphilis, M.L., Zhao, Y., Zhang, J., Burgers, P.M., Crouch, R.J., and Cerritelli, S.M. (2009). Contributions of the two accessory subunits, RNASEH2B and RNASEH2C, to the activity and properties of the human RNase H2 complex. Nucleic Acids Res. *37*, 96–110.

Ciccia, A., and Elledge, S.J. (2010). The DNA damage response: making it safe to play with knives. Mol. Cell *40*, 179–204.

Clarke, A.R., Purdie, C.A., Harrison, D.J., Morris, R.G., Bird, C.C., Hooper, M.L., and Wyllie, A.H. (1993). Thymocyte apoptosis induced by p53-dependent and independent pathways. Nature *362*, 849–852.

Clayton, D.A. (2003). Mitochondrial DNA replication: what we know. IUBMB Life *55*, 213–217.

Crow, Y.J., Leitch, A., Hayward, B.E., Garner, A., Parmar, R., Griffith, E., Ali, M., Semple, C., Aicardi, J., Babul-Hirji, R., et al. (2006a). Mutations in genes encoding ribonuclease H2 subunits cause Aicardi-Goutières syndrome and mimic congenital viral brain infection. Nat. Genet. *38*, 910–916.

Crow, Y.J., Hayward, B.E., Parmar, R., Robins, P., Leitch, A., Ali, M., Black, D.N., van Bokhoven, H., Brunner, H.G., Hamel, B.C., et al. (2006b). Mutations in the gene encoding the 3′-5′ DNA exonuclease TREX1 cause Aicardi-Goutières syndrome at the AGS1 locus. Nat. Genet. *38*, 917–920.

Crow, Y.J., and Rehwinkel, J. (2009). Aicardi-Goutieres syndrome and related phenotypes: linking nucleic acid metabolism with autoimmunity. Hum. Mol. Genet. *18*(R2), R130–R136.

Eder, P.S., Walder, R.Y., and Walder, J.A. (1993). Substrate specificity of human RNase H1 and its role in excision repair of ribose residues misincorporated in DNA. Biochimie *75*, 123–126.

El Hage, A., French, S.L., Beyer, A.L., and Tollervey, D. (2010). Loss of Topoisomerase I leads to R-loop-mediated transcriptional blocks during ribosomal RNA synthesis. Genes Dev. *24*, 1546–1558.

Esposito, G., Godindagger, I., Klein, U., Yaspo, M.L., Cumano, A., and Rajewsky, K. (2000). Disruption of the Rev3l-encoded catalytic subunit of polymerase zeta in mice results in early embryonic lethality. Curr. Biol. *10*, 1221–1224.

Figiel, M., Chon, H., Cerritelli, S.M., Cybulska, M., Crouch, R.J., and Nowotny, M. (2011). The structural and biochemical characterization of human RNase H2 complex reveals the molecular basis for substrate recognition and Aicardi-Goutières syndrome defects. J. Biol. Chem. *286*, 10540–10550.

Förstemann, K., and Lingner, J. (2005). Telomerase limits the extent of base pairing between template RNA and telomeric DNA. EMBO Rep. *6*, 361–366.

Friedel, R.H., Seisenberger, C., Kaloff, C., and Wurst, W. (2007). EUCOMM–the European conditional mouse mutagenesis program. Brief. Funct. Genomics Proteomic. *6*, 180–185.

Goulian, M., Richards, S.H., Heard, C.J., and Bigsby, B.M. (1990). Discontinuous DNA synthesis by purified mammalian proteins. J. Biol. Chem. *265*, 18461–18471.

Grossman, L.I., Watson, R., and Vinograd, J. (1973). The presence of ribonucleotides in mature closed-circular mitochondrial DNA. Proc. Natl. Acad. Sci. USA *70*, 3339–3343.

Hogrefe, H.H., Hogrefe, R.I., Walder, R.Y., and Walder, J.A. (1990). Kinetic analysis of Escherichia coli RNase H using DNA-RNA-DNA/DNA substrates. J. Biol. Chem. *265*, 5561–5566.

Holt, I.J. (2009). Mitochondrial DNA replication and repair: all a flap. Trends Biochem. Sci. *34*, 358–365.

Huertas, P., and Aguilera, A. (2003). Cotranscriptionally formed DNA:RNA hybrids mediate transcription elongation impairment and transcription-associated recombination. Mol. Cell *12*, 711–721.

Jeong, H.S., Backlund, P.S., Chen, H.C., Karavanov, A.A., and Crouch, R.J. (2004). RNase H2 of Saccharomyces cerevisiae is a complex of three proteins. Nucleic Acids Res. *32*, 407–414.

Joyce, C.M. (1997). Choosing the right sugar: how polymerases select a nucleotide substrate. Proc. Natl. Acad. Sci. USA *94*, 1619–1622.

Kasiviswanathan, R., and Copeland, W.C. (2011). Ribonucleotide discrimination and reverse transcription by the human mitochondrial DNA polymerase. J. Biol. Chem. *286*, 31490–31500.

Kim, N., Huang, S.N., Williams, J.S., Li, Y.C., Clark, A.B., Cho, J.E., Kunkel, T.A., Pommier, Y., and Jinks-Robertson, S. (2011). Mutagenic processing of ribonucleotides in DNA by yeast topoisomerase I. Science *332*, 1561–1564.

Kimura, S.H., Ikawa, M., Ito, A., Okabe, M., and Nojima, H. (2001). Cyclin G1 is involved in G2/M arrest in response to DNA damage and in growth control after damage recovery. Oncogene *20*, 3290–3300.

Kunkel, T.A., and Burgers, P.M. (2008). Dividing the workload at a eukaryotic replication fork. Trends Cell Biol. *18*, 521–527.

Lazzaro, F., Novarina, D., Amara, F., Watt, D.L., Stone, J.E., Costanzo, V., Burgers, P.M., Kunkel, T.A., Plevani, P., and Muzi-Falconi, M. (2012). RNase H and postreplication repair protect cells from ribonucleotides incorporated in DNA. Mol. Cell *45*, 99–110.

Li, X., and Manley, J.L. (2005). Inactivation of the SR protein splicing factor ASF/SF2 results in genomic instability. Cell *122*, 365–378.

Li, Y.F., and Breaker, R.R. (1999). Kinetics of RNA degradation by specific base catalysis of transesterification involving the 2 ′-hydroxyl group. J. Am. Chem. Soc. *121*, 5364–5372.

Lindahl, T., and Barnes, D.E. (2000). Repair of endogenous DNA damage. Cold Spring Harb. Symp. Quant. Biol. *65*, 127–133.

Lipkin, D., Talbert, P.T., and Cohn, M. (1954). The Mechanism of the Alkaline Hydrolysis of Ribonucleic Acids. J. Am. Chem. Soc. *76*, 2871–2872.

Mac Auley, A., Werb, Z., and Mirkes, P.E. (1993). Characterization of the unusually rapid cell cycles during rat gastrulation. Development *117*, 873–883.

Machida, Y., Okazaki, T., and Okazaki, R. (1977). Discontinuous replication of replicative form DNA from bacteriophage phiX174. Proc. Natl. Acad. Sci. USA *74*, 2776–2779.

Manel, N., and Littman, D.R. (2011). Hiding in plain sight: how HIV evades innate immune responses. Cell *147*, 271–274.

Miyabe, I., Kunkel, T.A., and Carr, A.M. (2011). The major roles of DNA polymerases epsilon and delta at the eukaryotic replication fork are evolutionarily conserved. PLoS Genet. *7*, e1002407.

Nick McElhinny, S.A., Kumar, D., Clark, A.B., Watt, D.L., Watts, B.E., Lundström, E.B., Johansson, E., Chabes, A., and Kunkel, T.A. (2010a). Genome instability due to ribonucleotide incorporation into DNA. Nat. Chem. Biol. *6*, 774–781.

Nick McElhinny, S.A., Watts, B.E., Kumar, D., Watt, D.L., Lundström, E.B., Burgers, P.M., Johansson, E., Chabes, A., and Kunkel, T.A. (2010b). Abundant ribonucleotide incorporation into DNA by yeast replicative polymerases. Proc. Natl. Acad. Sci. USA *107*, 4949–4954.

Norppa, H., and Falck, G.C. (2003). What do human micronuclei contain? Mutagenesis *18*, 221–233.

Nowotny, M., Gaidamakov, S.A., Ghirlando, R., Cerritelli, S.M., Crouch, R.J., and Yang, W. (2007). Structure of human RNase H1 complexed with an RNA/DNA hybrid: insight into HIV reverse transcription. Mol. Cell *28*, 264–276.

Pohjoismäki, J.L., Holmes, J.B., Wood, S.R., Yang, M.Y., Yasukawa, T., Reyes, A., Bailey, L.J., Cluett, T.J., Goffart, S., Willcox, S., et al. (2010). Mammalian mitochondrial DNA replication intermediates are essentially duplex but contain extensive tracts of RNA/DNA hybrid. J. Mol. Biol. *397*, 1144–1155.

Ramantani, G., Kohlhase, J., Hertzberg, C., Innes, A.M., Engel, K., Hunger, S., Borozdin, W., Mah, J.K., Ungerath, K., Walkenhorst, H., et al. (2010). Expanding the phenotypic spectrum of lupus erythematosus in Aicardi-Goutières syndrome. Arthritis Rheum. *62*, 1469–1477.

Reijns, M.A., Bubeck, D., Gibson, L.C., Graham, S.C., Baillie, G.S., Jones, E.Y., and Jackson, A.P. (2011). The structure of the human RNase H2 complex defines key interaction interfaces relevant to enzyme function and human disease. J. Biol. Chem. *286*, 10530–10539.

Rice, G., Patrick, T., Parmar, R., Taylor, C.F., Aeby, A., Aicardi, J., Artuch, R., Montalto, S.A., Bacino, C.A., Barroso, B., et al. (2007). Clinical and molecular phenotype of Aicardi-Goutieres syndrome. Am. J. Hum. Genet. *81*, 713–725.

Rice, G.I., Bond, J., Asipu, A., Brunette, R.L., Manfield, I.W., Carr, I.M., Fuller, J.C., Jackson, R.M., Lamb, T., Briggs, T.A., et al. (2009). Mutations involved in Aicardi-Goutières syndrome implicate SAMHD1 as regulator of the innate immune response. Nat. Genet. *41*, 829–832.

Rogakou, E.P., Pilch, D.R., Orr, A.H., Ivanova, V.S., and Bonner, W.M. (1998). DNA double-stranded breaks induce histone H2AX phosphorylation on serine 139. J. Biol. Chem. *273*, 5858–5868.

Rossi, M.L., and Bambara, R.A. (2006). Reconstituted Okazaki fragment processing indicates two pathways of primer removal. J. Biol. Chem. *281*, 26051–26061.

Rumbaugh, J.A., Murante, R.S., Shi, S., and Bambara, R.A. (1997). Creation and removal of embedded ribonucleotides in chromosomal DNA during mammalian Okazaki fragment processing. J. Biol. Chem. *272*, 22591–22599.

Rydberg, B., and Game, J. (2002). Excision of misincorporated ribonucleotides in DNA by RNase H (type 2) and FEN-1 in cell-free extracts. Proc. Natl. Acad. Sci. USA *99*, 16654–16659.

Satoh, M.S., and Lindahl, T. (1992). Role of poly(ADP-ribose) formation in DNA repair. Nature *356*, 356–358.

Shaban, N.M., Harvey, S., Perrino, F.W., and Hollis, T. (2010). The structure of the mammalian RNase H2 complex provides insight into RNA.NA hybrid processing to prevent immune dysfunction. J. Biol. Chem. *285*, 3617–3624.

Snow, M.H.L. (1977). Gastrulation in the mouse - growth and regionalization of epiblast. J. Embryol. Exp. Morphol. *42*, 293–303.

Stein, H., and Hausen, P. (1969). Enzyme from calf thymus degrading the RNA moiety of DNA-RNA Hybrids: effect on DNA-dependent RNA polymerase. Science *166*, 393–395.

Stetson, D.B., Ko, J.S., Heidmann, T., and Medzhitov, R. (2008). Trex1 prevents cell-intrinsic initiation of autoimmunity. Cell *134*, 587–598.

Tang, M.S., Bohr, V.A., Zhang, X.S., Pierce, J., and Hanawalt, P.C. (1989). Quantification of aminofluorene adduct formation and repair in defined DNA sequences in mammalian cells using the UVRABC nuclease. J. Biol. Chem. *264*, 14455–14462.

Testa, G., Schaft, J., van der Hoeven, F., Glaser, S., Anastassiadis, K., Zhang, Y., Hermann, T., Stremmel, W., and Stewart, A.F. (2004). A reliable lacZ expression reporter cassette for multipurpose, knockout-first alleles. Genesis *38*, 151–158.

Tibbetts, R.S., Brumbaugh, K.M., Williams, J.M., Sarkaria, J.N., Cliby, W.A., Shieh, S.Y., Taya, Y., Prives, C., and Abraham, R.T. (1999). A role for ATR in the DNA damage-induced phosphorylation of p53. Genes Dev. *13*, 152–157.

Turchi, J.J., Huang, L., Murante, R.S., Kim, Y., and Bambara, R.A. (1994). Enzymatic completion of mammalian lagging-strand DNA replication. Proc. Natl. Acad. Sci. USA *91*, 9803–9807.

Vengrova, S., and Dalgaard, J.Z. (2004). RNase-sensitive DNA modification(s) initiates S. pombe mating-type switching. Genes Dev. *18*, 794–804.

Vengrova, S., and Dalgaard, J.Z. (2006). The wild-type Schizosaccharomyces pombe mat1 imprint consists of two ribonucleotides. EMBO Rep. *7*, 59–65.

Ward, I.M., and Chen, J. (2001). Histone H2AX is phosphorylated in an ATR-dependent manner in response to replicational stress. J. Biol. Chem. *276*, 47759–47762.

Watt, D.L., Johansson, E., Burgers, P.M., and Kunkel, T.A. (2011). Replication of ribonucleotide-containing DNA templates by yeast replicative polymerases. DNA Repair (Amst.) *10*, 897–902.

Wittschieben, J., Shivji, M.K., Lalani, E., Jacobs, M.A., Marini, F., Gearhart, P.J., Rosewell, I., Stamp, G., and Wood, R.D. (2000). Disruption of the developmentally regulated Rev3l gene causes embryonic lethality. Curr. Biol. *10*, 1217–1220.

Yajima, H., Lee, K.J., and Chen, B.P. (2006). ATR-dependent phosphorylation of DNA-dependent protein kinase catalytic subunit in response to UV-induced replication stress. Mol. Cell. Biol. *26*, 7520–7528.

Yang, Y.G., Lindahl, T., and Barnes, D.E. (2007). Trex1 exonuclease degrades ssDNA to prevent chronic checkpoint activation and autoimmune disease. Cell *131*, 873–886.